

Direct multi-model dark-matter search with gravitational-wave interferometers using data from the first part of the fourth LIGO-Virgo-KAGRA observing run

The LIGO Scientific Collaboration, The Virgo Collaboration, and The KAGRA Collaboration*
(Dated: November 3, 2025)

Gravitational-wave detectors can probe the existence of dark matter with exquisite sensitivity. Here, we perform a search for three kinds of dark matter – dilatons (spin-0), dark photons (spin-1) and tensor bosons (spin-2) – using three independent methods on the first part of the most recent data from the fourth observing run of LIGO–Virgo–KAGRA. Each form of dark matter could have interacted with different standard-model particles in the instruments, causing unique differential strains on the interferometers. While we do not find any evidence for a signal, we place the most stringent upper limits to-date on each of these models. For scalars with masses between $[4 \times 10^{-14}, 1.5 \times 10^{-13}]$ eV that couple to photons or electrons, our constraints improve upon those from the third observing run by one order of magnitude, with the tightest limit of $\sim 10^{-20}$ GeV $^{-1}$ at a mass of $\sim 2 \times 10^{-13}$ eV. For vectors with masses between $[7 \times 10^{-13}, 8.47 \times 10^{-12}]$ eV that couple to baryons, our constraints supersede those from MICROSCOPE and Eöt-Wash by one to two orders of magnitude, reaching a minimum of $\sim 5 \times 10^{-24}$ at a mass of $\sim 10^{-12}$ eV. For tensors with masses of $[4 \times 10^{-14}, 8.47 \times 10^{-12}]$ eV (the full mass range analyzed) that couple via a Yukawa interaction, our constraints surpass those from fifth-force experiments by four to five orders of magnitude, achieving a limit as low as $\sim 8 \times 10^{-9}$ at $\sim 2 \times 10^{-13}$ eV. Our results show that gravitational-wave interferometers have become frontiers for new physics and laboratories for direct multi-model dark-matter detection.

I. INTRODUCTION

The existence of dark matter (DM) is well established, yet its fundamental nature remains one of the most pressing mysteries in modern physics [1]. Across a vast range of possible masses and interaction strengths, dark matter could take many forms – from particles with masses of $\mathcal{O}(10^{-22})$ eV, whose wave-like behavior spans galactic scales [2], to primordial black holes with masses comparable to stars [3–5]. Among these possibilities, ultralight dark matter with masses $m_{\text{DM}} \ll 1$ eV presents a particularly compelling scenario. Not only do high-energy theories, including string theory, naturally predict such particles, but their extraordinarily low mass also implies a quantum-mechanical coherence over macroscopic distances, effectively turning them into oscillating background fields. If these fields interact weakly with standard model particles, they could produce distinctive, nearly monochromatic signals detectable by precision experiments [6, 7].

Gravitational-wave (GW) detectors, such as LIGO, Virgo and KAGRA [8–10], have already reshaped astrophysics by measuring the signals from merging black holes and neutron stars [11–13]. But their extraordinary sensitivity also makes them powerful tools for probing fundamental physics beyond GWs [14–17]. The same precision that captures the faint signals from GWs could reveal subtle interactions between dark matter and ordinary matter, also placing these detectors at the frontier of searches for new physics. Along these lines, multiple searches for dilatons and dark photons have been per-

formed on previous GW data [18–22], resulting in stringent constraints on dilatons and dark photons.

In contrast to previous works, we explore here how GW detectors can be used to search for ultralight dark matter in various forms simultaneously: scalar fields (such as dilatons, which may induce oscillations in fundamental constants) [7, 23–25], vector fields (like dark photons, exerting weak oscillating forces on matter) [6], and massive tensor fields (closely resembling GWs but with a nonzero mass) [26–29]. Each of these candidates leaves a unique imprint on GW detectors, offering a new way to constrain – or perhaps discover – some of the most elusive dark matter candidates predicted by theory.

II. DARK MATTER INTERACTION MODELS

Cold, ultralight DM consists of an enormous number of extremely light particles, which motivates its treatment as a classical oscillating field. The angular frequency of this field is fixed by the ultralight DM mass: $\omega = m_{\text{DM}}c^2/\hbar$; however, there is a small, stochastic frequency change caused by the Maxwell-Boltzmann velocity distribution of the DM particles: $\Delta\omega/\omega \sim v_0^2/c^2 \sim 10^{-6}$, where v_0 is the virial velocity of DM around the center of the galaxy. This frequency spread implies that the signal has a finite coherence time, of $\mathcal{O}(10^4)$ s at $m_{\text{DM}} \sim 10^{-12}$ eV, in which the signal can be treated as purely monochromatic, but spreads over $\Delta\omega$ if observing for longer than the coherence time. Likewise, the finite coherence time implies a finite coherence length, which greatly exceeds the separation of earth-based interferometers. Taken together, the finite coherence time and length indicate that the ultralight DM signal is narrow-band, stochastic and correlated, regardless of the ultra-

* Full author list given at the end of the article.

light DM model considered.

The following subsections consider the physics of each type of DM, and how it interacts with GW interferometers.

A. Scalar, dilaton dark matter

Models of ultralight dark matter predict that it could have originated through a vacuum misalignment mechanism in the early universe, and would manifest today as a coherently oscillating scalar field [24]. The coupling of such DM would effectively induce an oscillation of the values of fundamental constants, namely the electron rest mass and the fine structure constant, thus leading to the expansion and contraction of solids. When a field gradient exists, objects can also be accelerated. Many ideas have been proposed to detect such effects [30–33], with the current strongest direct constraints coming from experiments looking for the oscillation of fundamental constants using atomic clocks or spectroscopy [34–45]. More recently, several coupling paths were discovered to detect those same oscillations using gravitational-wave interferometers [7, 23–25, 46, 47]. The potential for DM-induced acceleration of the arm mirrors was used to derive upper limits in LIGO data [21], while oscillations in the size of the beamsplitter was used with the GEO600 detector [20] and the Fermilab holometer [48]. An additional coupling path through arm mirror size oscillations was discovered and used in [22, 49], and is used in this study.

Considering a simple linear expansion to the Standard Model Lagrangian \mathcal{L} , we can write the scalar field ϕ as [20]:

$$\mathcal{L} \supset \frac{\phi}{\Lambda_\gamma} \frac{F_{\mu\nu} F^{\mu\nu}}{4} - \frac{\phi}{\Lambda_e} m_e \bar{\psi}_e \psi_e, \quad (1)$$

where, $F_{\mu\nu}$ is the electromagnetic field tensor, ψ_e and $\bar{\psi}_e$ are the standard-model electron field and its Dirac conjugate, respectively, m_e is the electron rest-mass, and Λ_γ and Λ_e denote the scalar DM coupling constants to the photon and electron, respectively. We can see that when the Λ_i^{-1} is non-zero, the DM field induces changes in m_e and the fine structure constant α through $F_{\mu\nu}$. In turn, this modulates the sizes and refractive indices of solids.

In LIGO, by considering only oscillations in the size of the beamsplitter and test arm mirrors, we can relate the measured strain $h(\omega)$ to the aforementioned DM coupling constants as [22]:

$$h(f_0) \approx \left(\frac{1}{\Lambda_\gamma} + \frac{1}{\Lambda_e} \right) \frac{c \sqrt{2 \rho_{\text{DM}}}}{2\pi f_0} \frac{1}{A_{\text{cal}}(f_0)}, \quad (2)$$

where $\rho_{\text{DM}} = 0.4 \text{ GeV cm}^{-3}$ is the local DM energy density according to the standard galactic DM halo model [50] and $f_0 = \omega/(2\pi)$ is the DM frequency. A_{cal} , see Section A, is obtained through detailed optical simulations that account for finite light travel time effects [47], and encodes the interferometer response to scalar DM [22].

B. Vector dark photon dark matter

Spin-1 dark photons¹ could completely explain the relic abundance of DM [52]. These particles could arise from the misalignment mechanism [53–55], parametric resonance or the tachyonic instability of a scalar field [56–59], or from cosmic string network decays [60]. The observable effect would result from a coupling of dark photons to standard-model particles – either baryons or baryon minus leptons. In particular, this interaction would cause “dark” force on the mirrors, causing them to oscillate at a frequency fixed by the mass of the dark photon [6, 61].

The Lagrangian \mathcal{L} that characterizes the dark photon coupling to a number current density J^μ of baryons or baryons minus leptons is:

$$\mathcal{L} = -\frac{1}{4\mu_0} F^{\mu\nu} F_{\mu\nu} + \frac{1}{2\mu_0} \left(\frac{m_{\text{DM}} c}{\hbar} \right)^2 A^\mu A_\mu - \epsilon e J^\mu A_\mu, \quad (3)$$

where μ_0 is the magnetic permeability in vacuum, e is the electron charge, A_μ is the dark four-vector potential, and ϵ is the strength of the particle/dark photon coupling normalized by the electromagnetic coupling constant.

The strain on the interferometers caused by a dark photon DM signal is [6, 47]:

$$\begin{aligned} \sqrt{\langle h_{\text{D}}^2 \rangle} &= \frac{\sqrt{2}}{3} \frac{Q}{M} \frac{\hbar e}{c^4 \sqrt{\epsilon_0}} \sqrt{2 \rho_{\text{DM}}} v_0 \frac{\epsilon}{f_0}, \\ &\simeq 6.56 \times 10^{-26} \left(\frac{\epsilon}{10^{-22}} \right) \left(\frac{100 \text{ Hz}}{f_0} \right), \end{aligned} \quad (4)$$

where ϵ_0 is the permittivity of free space, Q/M is the charge-to-mass ratio of the mirrors in LIGO and $\omega = 2\pi f_0$. We take $Q/M = m_p^{-1}$, where $m_p = 0.93827 \text{ GeV}/c^2$ is the proton rest mass [62].

A second strain also appears because light takes a finite amount of time to travel between the input and end mirrors in the interferometer, during which the mirrors have moved in response to the ultralight DM field [47]:

$$\begin{aligned} \sqrt{\langle h_{\text{C}}^2 \rangle} &= \frac{\sqrt{3}}{2} \sqrt{\langle h_{\text{D}}^2 \rangle} \frac{2\pi f_0 L}{v_0}, \\ &\simeq 6.58 \times 10^{-25} \left(\frac{\epsilon}{10^{-22}} \right), \end{aligned} \quad (5)$$

where $L = 4 \text{ km}$ is the arm-length of the LIGO interferometers. The total strain is: $\langle h_{\text{total}}^2 \rangle = \langle h_{\text{D}}^2 \rangle + \langle h_{\text{C}}^2 \rangle$. The averages are taken over polarization direction, detector geometry, and the Maxwell-Boltzmann velocity distribution.

¹ These dark photons are different than those that kinetically mix with the ordinary photon [51].

C. Tensor dark matter

A novel massive spin-2 particle, derived from a massive gravity theory, could modify gravity and emerge as a promising DM candidate. The foundational framework for linear massive gravity was established by Fierz and Pauli in 1939 [63]. This theory was extended to the nonlinear level, enabling the incorporation of massive gravitons. However, this generalization introduced a non-stable degree of freedom known as the Boulware-Deser ghost [64]. To address this issue, a ghost-free massive gravity theory was constructed [65, 66], which later evolved into the bimetric gravity [67] and multigravity theories [68]. In particular, in bimetric gravity [67, 69], two spin-2 particles produced by the misalignment mechanism [30] – one massless and one massive – could interact and explain DM [27].

The Fierz-Pauli Lagrangian density [70] describes this tensor field $\chi_{\mu\nu}$:

$$\mathcal{L} = -\frac{1}{4}\chi^{\mu\nu}\mathcal{E}_{\mu\nu,\alpha\beta}\chi^{\alpha\beta} - \frac{1}{8}\left(\frac{m_{\text{DM}}c}{\hbar}\right)^2(\chi_{\mu\nu}\chi^{\mu\nu} - \chi^2), \quad (6)$$

where $\chi \equiv \chi_{\mu}^{\mu}$ and $\mathcal{E}_{\mu\nu,\alpha\beta}$ is a second-order derivative operator defined in Eq. 2.13 of [26].

Using the Friedman-Lemaitre-Robertson-Walker (FLRW) background metric, one can derive the equations of motion for this ultralight field at late times in the universe [27, 71, 72].

The strain on interferometers arises analogously to that from GWs: a stretching of space-time in the presence of the field, since the massive spin-2 metric and its coupling constant can be absorbed into the definition of the massless spin-2 metric in the linear regime of the coupling constant α ; thus, the strain can be derived [26, 29]²:

$$h(f_0) = \frac{2\alpha\Delta\varepsilon}{2\pi f_0 m_{\text{Pl}}}\sqrt{\frac{\rho_{\text{DM}}\hbar c}{2}} \simeq 1.23 \times 10^{-25} \left(\frac{\alpha}{5 \times 10^{-8}}\right) \left(\frac{100 \text{ Hz}}{f_0}\right) \quad (7)$$

where $\Delta\varepsilon := \varepsilon_{ij}(n^i n^j - m^i m^j)$, n, m are unit vectors pointing down each interferometer arm, ε_{ij} describes each of the five polarizations of the ultralight DM field [28], α is the Yukawa coupling, and m_{Pl} is the reduced Planck mass.

² Note that Refs. [26, 29] and Refs. [27, 28] differ by a factor of 2 in the strain induced by tensor DM, which results from a factor of 8 difference in the Lagrangians. We use the prescriptions in [26, 29] throughout this paper, which leads to a factor of two stronger upper limits than would be obtained using the formalism of [27, 28]

III. DATA

We analyze data from the first part of the fourth observing run (O4a) of the LIGO Livingston (L1) and Hanford (H1) detectors. The sensitivity of the detectors in this observing run improved significantly across all frequencies, particularly above 400 Hz [73–75]. The strain data were collected between May 24, 2023, at 15:00 UTC, and January 16, 2024, at 16:00 UTC, with L1 and H1 operating 69.0% and 67.5% of the time, respectively [76]. Virgo was not operational during O4a, and KAGRA only observed for one month. The data are calibrated by directing a laser onto the test masses and comparing the measured response to the expected one [77, 78]. Additionally, the data have been cleaned to remove short-duration disturbances (known as “glitches”) [79], and are only analyzed if they are in “science mode” [80]. At worst, amplitude and phase uncertainties at 1σ are 10% and 10 degrees, respectively, between the frequency range analyzed by all methods: [10, 2000] Hz.

In this analysis, we use three independent pipelines, described in detail in Section IV, to search for direct DM interactions with GW interferometers. Each one employs data in different formats. The first, called the *BSD-excess-power* method, uses Band Sampled Data (BSD) structures [81] as the input to this search, which are derived from short fast Fourier transform databases [82]. BSDs contain complex-valued time-series representations of the data every 10 Hz every month, and are derived from the strain channel `GDS-CALIB-STRAIN-CLEAN_AR`. The other two methods, *cross-correlation* and Logarithmic Power Spectral Density (*LPSD*), use *gated*³ data from the channel `GDS-CALIB-STRAIN-CLEAN_GATED_G02`, in which spurious glitches have been removed. The *cross-correlation* method employs 1800-s long short Fourier transforms (SFTs) created from G02 gated data during the O4a period for H1 and L1. In total, 5696 pairs of coincident SFTs for H1 and L1 were used, corresponding to a total of 2848 hours. In contrast, the data used by *LPSD* were divided in continuous segments of at least 1×10^5 s each, resulting in 30 segments totaling about 1157 h, similarly to [22].

IV. SEARCH METHODS

We present three different methods that searched for ultralight DM coupling to the interferometers. All methods are sensitive to each kind of DM presented in Section II.

³ Gating refers to removing the cumulative effect of many loud, transient glitches that can collectively raise the noise floor and inhibit the recovery of CW signals.

A. Cross-Correlation

The effect of a large population of ultralight dark photons on the interferometers is similar to a stochastic GW background, and the long coherence length of the field, e.g. $\mathcal{O}(10^9)$ m at $m_{\text{DM}} = 10^{-12}$ eV [6, 61], is much larger than the separation between H1 and L1, both of which motivate a *cross-correlation* search. Additionally, the velocity spread of the dark photon field leads to a very narrow relative frequency spread of the order $\sim 10^{-6}$ for the signal, leading naturally to a frequency-domain peak hunt in each frequency bin of size 1/1800 Hz (see [18, 19] for previous searches with O1 and O3 data). The signal-to-noise ratio (SNR) for the frequency bin j is defined as

$$\text{SNR}_j = \frac{S_j}{\sigma_j}. \quad (8)$$

Here the signal part S_j is the signal strength constructed by cross-correlating the FFT data $z_{1,ij}$ and $z_{2,ij}$ of detectors 1 and 2 for segment i , and averaging over the segments:

$$S_j = \frac{1}{N_{\text{FFT}}} \sum_{i=1}^{N_{\text{FFT}}} \frac{z_{1,ij} z_{2,ij}^*}{P_{1,ij} P_{2,ij}}, \quad (9)$$

where $P_{1(2),ij}$ is the noise power estimated from the neighboring 50 frequency bins⁴ using a running median, and is related to the one-sided power spectral density (PSD) by $\text{PSD}_{1(2),ij} = 2P_{1(2),ij}/T_{\text{FFT}}$. In the absence of a signal, the expectation value of S_j is zero, with a variance for its real and imaginary parts being

$$\sigma_j^2 = \frac{1}{N_{\text{FFT}}} \left\langle \frac{1}{2P_{1,ij} P_{2,ij}} \right\rangle_{N_{\text{FFT}}}. \quad (10)$$

The length T_{FFT} of each time segment is 1800s, and an efficiency factor obtained from simulations is used to correct for the power loss due to this binning choice and random bin boundary when the calculated SNR is converted to upper limits [18]. In the presence of the dark photons, the SNR thus defined takes a negative and real value due to the relative orientation of the two detectors which results in a negative overlap reduction function, close to -0.9 for the entire frequency range we consider here, and is used in converting the SNR at each frequency bin to an upper limit. In the search for the candidate, bins that are contaminated by narrow spectral artifacts, defined to be within ~ 0.056 Hz, are excluded in the analysis. The upper limits are derived with the Feldman-Cousins formalism [83] in the absence of a detection.

⁴ Fifty bins ensures that the signal does not pollute the background estimation and the noise properties do not differ by too much across the frequency range of the estimation.

B. BSD excess power method

In each 1-Hz band, *BSD-excess-power* changes the fast Fourier transform coherence time T_{FFT} to match the DM signal coherence time T_{coh} ensuring that all power is confined to one frequency bin for the full observing run. We then take Fourier transforms of the strain data with durations T_{FFT} to make time-frequency “peakmaps” [82, 84]. “Peakmaps” are collections of ones that represent when the power in particular frequency bins has exceeded a threshold in the equalized spectrum and is also a local maxima. We then count the number of peaks at each frequency to find bins with large numbers of peaks. By summing the ones in the peakmap, and not the actual power in each frequency bin, we are more robust against non-Gaussian noise artifacts that could contaminate particular frequency bins and bias our detection statistic.

We define the critical ratio CR to be our detection statistic:

$$CR = \frac{y - \mu}{\sigma}, \quad (11)$$

where y is the number of peaks at a particular frequency, and μ and σ are the mean and standard deviations of the number counts across all frequencies in the band. In Gaussian noise, the CR is approximately normally distributed with zero mean and unit variance, and approximately a normalized non-central χ^2 distribution with two degrees of freedom in the presence of a signal.

We select enough candidates⁵ in each 1-Hz band such that one coincident candidate between two detectors would occur in Gaussian noise. This ensures that we select uniformly over the frequency range.

C. LPSD

The crux of the *LPSD* approach is to exactly match the integration time in Fourier transforms to the DM coherence time in every bin. This allows it to maximize the SNR to a theoretical maximum. The resulting necessary logarithmic frequency spacing in this method poses a challenge as FFT-based algorithms are no longer applicable. With a computational complexity scaling as $\mathcal{O}(N^2)$, where N is the number of data points, this appears to lead to intractable costs. In [49], a method was developed that leverages symmetries between the time and frequency domains. This allows us to perform the full logarithmic calculation with a single FFT followed by a heavily zero-suppressed transformation without the need for an expensive pre-computation.

Having efficiently calculated PSDs over large segments of data with this method, we follow the approach in [22, 49]

⁵ The number of candidates selected ranges from 20 and 285 at 2000 Hz and 10 Hz, respectively and depends on T_{FFT} .

where, similar to LIGO calibration, a background model is constructed by fitting cubic splines in log-log space to the PSD as a function of frequency. Because the PSDs vary by several orders of magnitude, we conduct fits over intervals of 10^4 frequency bins. Within these intervals, potential DM signals are identified as positive deviations from the fits by using a profile likelihood test (see Eq. 15 in [49]) assuming, as validated empirically, that the residuals follow a skew-normal distribution.

V. RESULTS

A. Cross-Correlation

With the definition of the SNR (Eq. (8)), the desired candidate needs to satisfy $\text{Re}(\text{SNR}) < -5.8$ to correspond to a detection with an overall $\sim 1\%$ false alarm probability. No such candidate was found in this analysis. We have also checked the subthreshold outliers with absolute values in the range $[5.0, 5.8]$ for either the real or imaginary part of the SNR. Of ten such outliers, nine are due to loud instrumental artifacts, and the remaining one is consistent with Gaussian noise.

In the absence of a detection, we then set 95% confidence-level upper limits on each of the aforementioned DM models in each frequency (or mass) bin, which induces fluctuations in the limits that are broader than those from the other methods, in which the limits are set roughly every one Hz.

B. BSD Excess power method

Our search returned 6847 candidates present in the same frequency bin in both L1 and H1 and that did not overlap with known noise disturbances [79]. However, after requiring that the average CR be greater than five (corresponding to 5σ significance in Gaussian noise), only ten candidates remained. To determine whether these candidates resulted from DM, we performed three follow-up procedures: (1) we varied the observation time T_{obs} at the chosen T_{FFT} to see if there was a steady increase in the $CR \propto T_{\text{obs}}^{1/2}$, (2) we increased $T_{\text{FFT}} > T_{\text{coh}}$ to see if there was a *decrease* in the CR [20, 61], and (3) we correlated the spectra from L1 and H1 with an expected DM waveform using the Wiener filter [85] and computed the residual between them [86]. No candidate survived all three follow-ups.

In the absence of candidates, we set upper limits on the minimum detectable strain amplitude at 95% confidence $h_{0,\text{min}}^{95\%}$ induced by a generic DM signal using Eq. 75 of [17], which depends on the detector power spectral density, the maximum of the coincident candidates' CRs , T_{FFT} , and T_{obs} . Up to an $\mathcal{O}(1)$ factor that depends on the DM polarization and the geometry of LIGO, these limits can then be mapped to *any* kind of DM interaction that would induce a differential strain on the detector.

C. LPSD

We obtain candidates by performing a profile likelihood ratio test in each bin, as outlined in [49], and require a 5σ significance corrected for the *look-elsewhere effect*⁶ in rejecting the no-DM hypothesis. After clustering neighboring bins, requiring significance and compatibility in both detectors, we find only one candidate which was found to originate from a non-optimal setting in the background fit.

The resulting 95% confidence-level upper limits on Λ_i^{-1} , where Λ_i is either Λ_e or Λ_γ (see Eq. (2)) when assuming the other is zero, can be seen in Fig. 1(a). As one can see, we improve on the O3 results by up to an order of magnitude over the entire frequency range. We note that the O3 curve in the plot is multiplied by a factor 2.226 compared to the results in [22] after we found a conversion error. The improvement at higher frequencies can be attributed to the better detector sensitivity in O4a. At lower frequencies, a larger arm mirror thickness difference compared to O3 leads to a roughly factor of three improvement, and the gating procedure – not used in the O3 search – leads to an improvement up to a factor of two. Injection tests were performed that confirmed the upper limits at the expected level, but found a systematic leading us to overestimate the limits by 13%. This is small compared to the 30% statistical uncertainty.

D. Upper limits

For all three pipelines, the follow-up steps, predetermined before analyzing the data, yielded no surviving candidates. Thus, we show in Fig. 1 upper limits for each of the three DM models using each pipeline, as argued in [17, 87]. For all three DM models, we see significant improvements in the constraints on the coupling constants with respect to existing experiments. For dark photons, *cross-correlation* obtains less stringent constraints than those from *BSD-excess-power* and *LPSD* because it is significantly less sensitive to the finite-light travel time effect [29, 47]. For dilatons, *cross-correlation* is consistent with or outperforms *BSD-excess-power* and *LPSD* because all three methods are equally sensitive to the finite light-travel time effect. For tensor bosons, the upper limits obtained by all three pipelines are consistent and significantly outperform fifth-force experiments by several orders of magnitude, as expected from [28, 88].

We note that the indirect fifth-force upper limits are stronger than those obtained from our search for scalar DM. In this case, the sensitivity of GW interferometers does not benefit significantly from the arm length, as

⁶ This effect arises because when searching over a large parameter space, noise has an increased opportunity to cause a false alarm somewhere in the space.

shown in the recent GEO600 search [20], where the relevant effect was the differential strain induced by the oscillating beam-splitter. Improvements by accounting for the different thicknesses of the test masses [22], together with the better low-frequency sensitivity of LIGO compared to GEO600 [89, 90], lead to substantial gains below 200 Hz relative to the GEO600 results, but still remain weaker than fifth-force constraints.

By contrast, the sensitivity to dark photons and tensor bosons in LIGO, Virgo and KAGRA depends primarily on the interferometer arm length, just as for GWs. In these cases, the differential strain induced by DM coupling to the test masses, or spacetime distortions from tensor fields, is amplified by the long arms, enhancing our sensitivity to these kinds of DM. In particular, for tensor bosons, a torsion balance responds as a single bulk object, analogous to early resonant-bar detectors, which are far less sensitive than interferometers [91]. Thus, the sensitivity of fifth-force experiments is strongest for scalars and weakens for vectors and tensors, while GW interferometers are more powerful probes of vectors and tensors than scalars.

VI. CONCLUSIONS

We have shown that it may be possible for GW interferometers to detect different kinds of DM – dilatons, dark photons and tensor bosons – using computationally efficient search techniques. Each form of DM interacts uniquely with the components of the interferometers, leading to signals that may be distinguishable. Though we have not found any evidence for DM in our searches, we have placed stringent upper limits on three DM models that improve over those of existing experiments by orders of magnitude. Specifically, for dilatons and dark photons, we continue to probe weaker and weaker couplings due to upgrades in GW interferometers and improvements in our analysis techniques; for tensor bosons, we surpass by five orders of magnitude fifth-force constraints for the first time. We note that all upper limits do not include an average of the Maxwell-Boltzmann distributed velocities, which is a conservative choice – such an average would result in the strengthening of the dark photon limits by a factor of $\sim \sqrt{3}/2$, though would not impact the other limits. In future work, we will consider more systematically the impact of the velocity distribution on the upper limits, which will likely lead to improvements in the dark photon limits. Thus, our results motivate treating LIGO, Virgo and KAGRA as highly precise DM detectors, permitting an unexpected way to probe new physics.

ACKNOWLEDGMENTS

This material is based upon work supported by NSF’s LIGO Laboratory, which is a major facility fully funded

by the National Science Foundation. The authors also gratefully acknowledge the support of the Science and Technology Facilities Council (STFC) of the United Kingdom, the Max-Planck-Society (MPS), and the State of Niedersachsen/Germany for support of the construction of Advanced LIGO and construction and operation of the GEO 600 detector. Additional support for Advanced LIGO was provided by the Australian Research Council. The authors gratefully acknowledge the Italian Istituto Nazionale di Fisica Nucleare (INFN), the French Centre National de la Recherche Scientifique (CNRS) and the Netherlands Organization for Scientific Research (NWO) for the construction and operation of the Virgo detector and the creation and support of the EGO consortium. The authors also gratefully acknowledge research support from these agencies as well as by the Council of Scientific and Industrial Research of India, the Department of Science and Technology, India, the Science & Engineering Research Board (SERB), India, the Ministry of Human Resource Development, India, the Spanish Agencia Estatal de Investigación (AEI), the Spanish Ministerio de Ciencia, Innovación y Universidades, the European Union NextGenerationEU/PRTR (PRTR-C17.I1), the ICSC - CentroNazionale di Ricerca in High Performance Computing, Big Data and Quantum Computing, funded by the European Union NextGenerationEU, the Comunitat Autònoma de les Illes Balears through the Conselleria d’Educació i Universitats, the Conselleria d’Innovació, Universitats, Ciència i Societat Digital de la Generalitat Valenciana and the CERCA Programme Generalitat de Catalunya, Spain, the Polish National Agency for Academic Exchange, the National Science Centre of Poland and the European Union - European Regional Development Fund; the Foundation for Polish Science (FNP), the Polish Ministry of Science and Higher Education, the Swiss National Science Foundation (SNSF), the Russian Science Foundation, the European Commission, the European Social Funds (ESF), the European Regional Development Funds (ERDF), the Royal Society, the Scottish Funding Council, the Scottish Universities Physics Alliance, the Hungarian Scientific Research Fund (OTKA), the French Lyon Institute of Origins (LIO), the Belgian Fonds de la Recherche Scientifique (FRS-FNRS), Actions de Recherche Concertées (ARC) and Fonds Wetenschappelijk Onderzoek - Vlaanderen (FWO), Belgium, the Paris Île-de-France Region, the National Research, Development and Innovation Office of Hungary (NKFIH), the National Research Foundation of Korea, the Natural Sciences and Engineering Research Council of Canada (NSERC), the Canadian Foundation for Innovation (CFI), the Brazilian Ministry of Science, Technology, and Innovations, the International Center for Theoretical Physics South American Institute for Fundamental Research (ICTP-SAIFR), the Research Grants Council of Hong Kong, the National Natural Science Foundation of China (NSFC), the Israel Science Foundation (ISF), the US-Israel Binational Science Fund (BSF), the Leverhulme Trust, the Research Corporation,

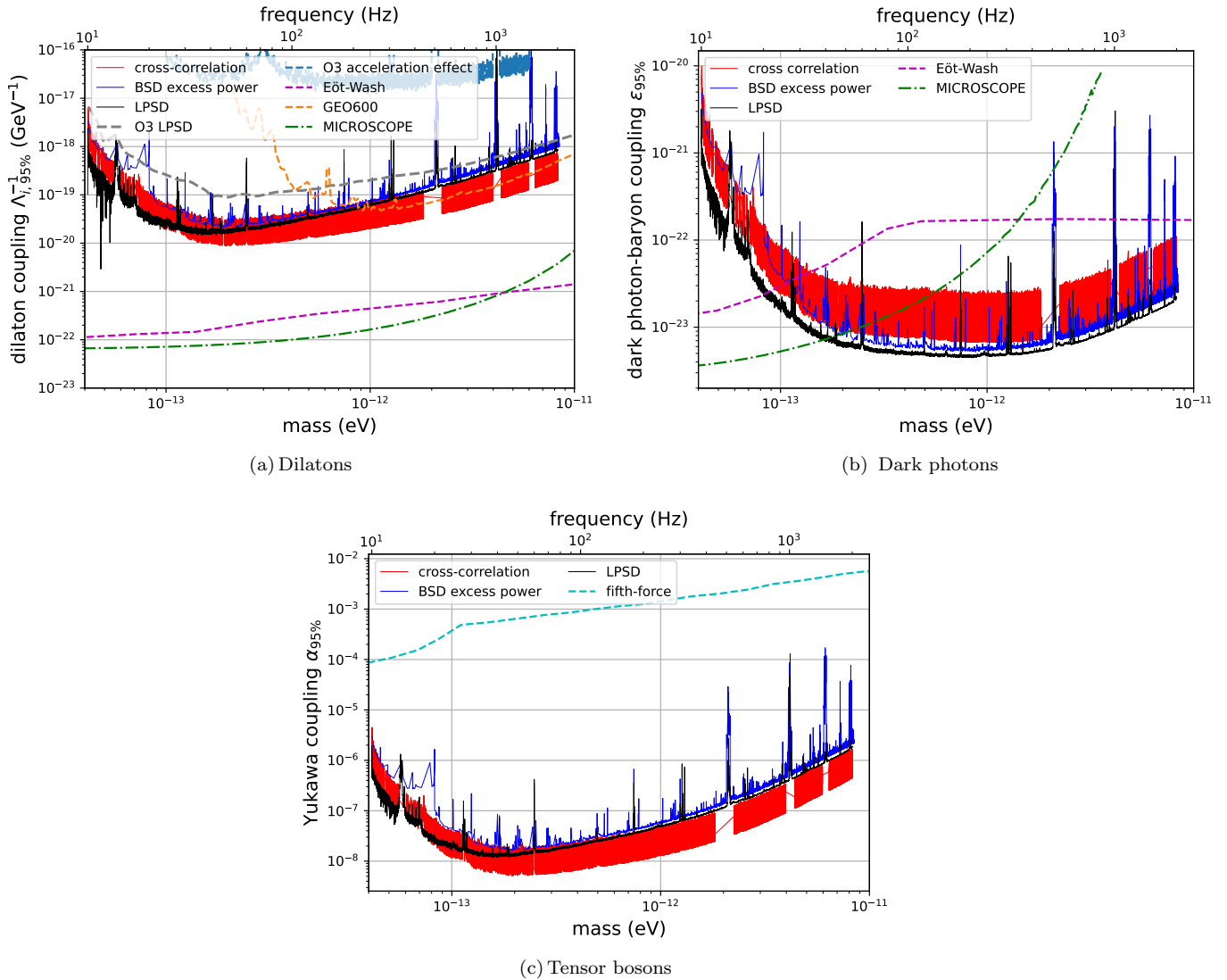


FIG. 1. **Upper limits on the coupling strengths of ultralight scalar, vector and tensor bosons to standard-model particles in LIGO.** Solid lines denote the constraints from this work (“cross-correlation,” “BSD excess power,” and “LPSD”). The dashed and dotted-dashed lines indicate constraints from other experiments (“Eöt-Wash” and “MICROSCOPE”) and from other searches on GW interferometer data (“GEO600,” “O3 LPSD” and “O3 acceleration effect”). (a) Our constraints apply to the coupling of dilatons to both photons and to electrons. They improve upon those from previous searches with GW interferometers [20–22] and beat those from O3 by one order of magnitude. Constraints from Eöt-Wash and MICROSCOPE correspond to the coupling of the dilaton to the electron. (b) The constraints on vector dark photon DM improve upon existing limits by a couple of order of magnitudes in the dark-photon/baryon coupling constant. To produce limits on dark photon/baryon minus lepton coupling, $U(1)_{B-L}$, these limits should be multiplied by two. (c) For the first time, we derive constraints on tensor DM using GW interferometers, which are up to five orders of magnitude superior to those obtained indirectly from fifth-force experiments [92, 93]. Note that for tensor bosons, using the calculated strain amplitudes in Refs. [27, 28] would require multiplying the limits on the tensor boson coupling constant by two.

the National Science and Technology Council (NSTC), Taiwan, the United States Department of Energy, and the Kavli Foundation. The authors gratefully acknowledge the support of the NSF, STFC, INFN and CNRS for provision of computational resources.

This work was supported by MEXT, the JSPS Leading-edge Research Infrastructure Program, JSPS

Grant-in-Aid for Specially Promoted Research 26000005, JSPS Grant-in-Aid for Scientific Research on Innovative Areas 2402: 24103006, 24103005, and 2905: JP17H06358, JP17H06361 and JP17H06364, JSPS Core-to-Core Program A. Advanced Research Networks, JSPS Grants-in-Aid for Scientific Research (S) 17H06133 and 20H05639, JSPS Grant-in-Aid for Transformative Re-

search Areas (A) 20A203: JP20H05854, the joint research program of the Institute for Cosmic Ray Research, University of Tokyo, the National Research Foundation (NRF), the Computing Infrastructure Project of the Global Science experimental Data hub Center (GSDC) at KISTI, the Korea Astronomy and Space Science Institute (KASI), the Ministry of Science and ICT (MSIT) in Korea, Academia Sinica (AS), the AS Grid Center (ASGC) and the National Science and Technology Council (NSTC) in Taiwan under grants including the Science Vanguard Research Program, the Advanced Technology

Center (ATC) of NAOJ, and the Mechanical Engineering Center of KEK.

Additional acknowledgements for support of individual authors may be found in the following document:

<https://dcc.ligo.org/LIGO-M2300033/public>. For the purpose of open access, the authors have applied a Creative Commons Attribution (CC BY) license to any Author Accepted Manuscript version arising. We request that citations to this article use 'A. G. Abac *et al.* (LIGO-Virgo-KAGRA Collaboration), ...' or similar phrasing, depending on journal convention.

-
- [1] G. Bertone and D. Hooper, *Rev. Mod. Phys.* **90**, 045002 (2018), arXiv:1605.04909 [astro-ph.CO].
- [2] E. G. M. Ferreira, *Astron. Astrophys. Rev.* **29**, 7 (2021), arXiv:2005.03254 [astro-ph.CO].
- [3] B. Carr, F. Kuhnel, and M. Sandstad, *Phys. Rev. D* **94**, 083504 (2016), arXiv:1607.06077 [astro-ph.CO].
- [4] B. Carr, S. Clesse, J. García-Bellido, and F. Kühnel, *Phys. Dark Univ.* **31**, 100755 (2021), arXiv:1906.08217 [astro-ph.CO].
- [5] A. M. Green and B. J. Kavanagh, *J. Phys. G* **48**, 043001 (2021), arXiv:2007.10722 [astro-ph.CO].
- [6] A. Pierce, K. Riles, and Y. Zhao, *Phys. Rev. Lett.* **121**, 061102 (2018), arXiv:1801.10161 [hep-ph].
- [7] H. Grote and Y. V. Stadnik, *Phys. Rev. Res.* **1**, 033187 (2019), arXiv:1906.06193 [astro-ph.IM].
- [8] J. Aasi, B. P. Abbott, R. Abbott, T. Abbott, M. R. Abernathy, K. Ackley, C. Adams, T. Adams, P. Addesso, and et al., *CQGra* **32**, 074001 (2015), arXiv:1411.4547 [gr-qc].
- [9] F. Acernese, M. Agathos, K. Agatsuma, D. Aisa, N. Allemandou, A. Allocca, J. Amarni, P. Astone, G. Balestri, G. Ballardín, and et al., *CQGra* **32**, 024001 (2015), arXiv:1408.3978 [gr-qc].
- [10] T. Akutsu *et al.* (KAGRA), *PTEP* **2021**, 05A101 (2021), arXiv:2005.05574 [physics.ins-det].
- [11] B. Abbott *et al.* (LIGO Scientific Collaboration, Virgo), *Phys. Rev. Lett.* **116**, 061102 (2016), arXiv:1602.03837 [gr-qc].
- [12] B. P. Abbott *et al.* (LIGO Scientific Collaboration and Virgo Collaboration), *Physical Review Letters* **119**, 161101 (2017).
- [13] R. Abbott *et al.* (LIGO Scientific Collaboration, Virgo, KAGRA), (2021), arXiv:2111.03606 [gr-qc].
- [14] A. Arvanitaki, M. Baryakhtar, and X. Huang, *Phys. Rev. D* **91**, 084011 (2015), arXiv:1411.2263 [hep-ph].
- [15] G. Bertone *et al.*, *SciPost Phys. Core* **3**, 007 (2020), arXiv:1907.10610 [astro-ph.CO].
- [16] Q. L. Nguyen and A. L. Miller, *PoS EPS-HEP2023*, 132 (2024).
- [17] A. L. Miller, (2025), arXiv:2503.02607 [astro-ph.HE].
- [18] H.-K. Guo, K. Riles, F.-W. Yang, and Y. Zhao, *Commun. Phys.* **2**, 155 (2019), arXiv:1905.04316 [hep-ph].
- [19] R. Abbott *et al.* (LIGO Scientific Collaboration, Virgo, KAGRA), *Phys. Rev. D* **105**, 063030 (2022), arXiv:2105.13085 [astro-ph.CO].
- [20] S. M. Vermeulen *et al.*, *Nature* **600**, 424 (2021).
- [21] K. Fukusumi, S. Morisaki, and T. Suyama, *Phys. Rev. D* **108**, 095054 (2023), arXiv:2303.13088 [hep-ph].
- [22] A. S. Göttel, A. Ejlli, K. Karan, S. M. Vermeulen, L. Aiello, V. Raymond, and H. Grote, *Phys. Rev. Lett.* **133**, 101001 (2024), arXiv:2401.18076 [astro-ph.CO].
- [23] Y. Stadnik and V. Flambaum, *Physical Review Letters* **114**, 161301 (2015).
- [24] Y. Stadnik and V. Flambaum, *Physical Review Letters* **115**, 201301 (2015).
- [25] Y. Stadnik and V. Flambaum, *Physical Review A* **93**, 063630 (2016).
- [26] K. Aoki and S. Mukohyama, *Phys. Rev. D* **94**, 024001 (2016), arXiv:1604.06704 [hep-th].
- [27] L. Marzola, M. Raidal, and F. R. Urban, *Phys. Rev. D* **97**, 024010 (2018), arXiv:1708.04253 [hep-ph].
- [28] J. M. Armaleo, D. L. Nacir, and F. R. Urban, *JCAP* **04**, 053 (2021), arXiv:2012.13997 [astro-ph.CO].
- [29] Y. Manita, H. Takeda, K. Aoki, T. Fujita, and S. Mukohyama, *Phys. Rev. D* **109**, 095012 (2024), arXiv:2310.10646 [hep-ph].
- [30] J. Preskill, M. B. Wise, and F. Wilczek, *Phys. Lett. B* **120**, 127 (1983).
- [31] L. Abbott and P. Sikivie, *Phys. Lett. B* **120**, 133 (1983).
- [32] M. Dine and W. Fischler, *Phys. Lett. B* **120**, 137 (1983).
- [33] Y. Cho and J. Kim, *Phys. Rev. D* **79**, 023504 (2009), arXiv:0711.2858 [gr-qc].
- [34] A. Arvanitaki, J. Huang, and K. Van Tilburg, *Phys. Rev. D* **91**, 015015 (2015), arXiv:1405.2925 [hep-ph].
- [35] S. Aharony, N. Akerman, R. Ozeri, G. Perez, I. Savoray, and R. Shaniv, *Phys. Rev. D* **103**, 075017 (2021), arXiv:1902.02788 [hep-ph].
- [36] E. Savalle, A. Hees, F. Frank, E. Cantin, P.-E. Pottie, B. M. Roberts, L. Cros, B. T. McAllister, and P. Wolf, *Phys. Rev. Lett.* **126**, 051301 (2021), arXiv:2006.07055 [gr-qc].
- [37] C. J. Kennedy, E. Oelker, J. M. Robinson, T. Bothwell, D. Kedar, W. R. Milner, G. E. Marti, A. Derivianko, and J. Ye, *Phys. Rev. Lett.* **125**, 201302 (2020), arXiv:2008.08773 [physics.atom-ph].
- [38] D. Antypas, O. Tretiak, A. Garcon, R. Ozeri, G. Perez, and D. Budker, *Phys. Rev. Lett.* **123**, 141102 (2019), arXiv:1905.02968 [physics.atom-ph].
- [39] D. Antypas, O. Tretiak, K. Zhang, A. Garcon, G. Perez, M. G. Kozlov, S. Schiller, and D. Budker, *Quantum Sci. Technol.* **6**, 034001 (2021), arXiv:2012.01519 [physics.atom-ph].
- [40] O. Tretiak, X. Zhang, N. L. Figueroa, D. Antypas, A. Brogna, A. Banerjee, G. Perez, and D. Budker, *Phys. Rev. Lett.* **129**, 031301 (2022), arXiv:2201.02042 [hep-ph].

- ph].
- [41] R. Oswald *et al.*, Phys. Rev. Lett. **129**, 031302 (2022), arXiv:2111.06883 [hep-ph].
- [42] W. M. Campbell, B. T. McAllister, M. Goryachev, E. N. Ivanov, and M. E. Tobar, Phys. Rev. Lett. **126**, 071301 (2021), arXiv:2010.08107 [hep-ex].
- [43] K. Beloy *et al.* (BACON), Nature **591**, 564 (2021), arXiv:2005.14694 [physics.atom-ph].
- [44] X. Zhang, A. Banerjee, M. Leyser, G. Perez, S. Schiller, D. Budker, and D. Antypas, Phys. Rev. Lett. **130**, 251002 (2023), arXiv:2212.04413 [physics.atom-ph].
- [45] N. Sherrill *et al.*, New J. Phys. **25**, 093012 (2023), arXiv:2302.04565 [physics.atom-ph].
- [46] S. Morisaki and T. Suyama, Phys. Rev. D **100**, 123512 (2019).
- [47] S. Morisaki, T. Fujita, Y. Michimura, H. Nakatsuka, and I. Obata, Phys. Rev. D **103**, L051702 (2021), arXiv:2011.03589 [hep-ph].
- [48] L. Aiello, J. W. Richardson, S. M. Vermeulen, H. Grote, C. Hogan, O. Kwon, and C. Stoughton, Phys. Rev. Lett. **128**, 121101 (2022), arXiv:2108.04746 [gr-qc].
- [49] A. Göttel and V. Raymond, (2025), arXiv:2503.03293 [astro-ph.CO].
- [50] J. I. Read, J. Phys. G **41**, 063101 (2014), arXiv:1404.1938 [astro-ph.GA].
- [51] B. Holdom, Phys. Lett. B **166**, 196 (1986).
- [52] P. Agrawal, N. Kitajima, M. Reece, T. Sekiguchi, and F. Takahashi, Phys. Lett. B **801**, 135136 (2020), arXiv:1810.07188 [hep-ph].
- [53] A. E. Nelson and J. Scholtz, Physical Review D **84**, 103501 (2011).
- [54] P. Arias, D. Cadamuro, M. Goodsell, J. Jaeckel, J. Redondo, and A. Ringwald, Journal of Cosmology and Astroparticle Physics **2012**, 013 (2012).
- [55] P. W. Graham, J. Mardon, and S. Rajendran, Physical Review D **93**, 103520 (2016).
- [56] P. Agrawal, N. Kitajima, M. Reece, T. Sekiguchi, and F. Takahashi, Physics Letters B **801**, 135136 (2020).
- [57] R. T. Co, A. Pierce, Z. Zhang, and Y. Zhao, Phys. Rev. D **99**, 075002 (2019), arXiv:1810.07196 [hep-ph].
- [58] M. Bastero-Gil, J. Santiago, L. Ubaldi, and R. Vega-Morales, JCAP **04**, 015 (2019), arXiv:1810.07208 [hep-ph].
- [59] J. A. Dror, K. Harigaya, and V. Narayan, Phys. Rev. D **99**, 035036 (2019), arXiv:1810.07195 [hep-ph].
- [60] A. J. Long and L.-T. Wang, Physical Review D **99**, 063529 (2019).
- [61] A. L. Miller *et al.*, Phys. Rev. D **103**, 103002 (2021), arXiv:2010.01925 [astro-ph.IM].
- [62] S. Navas *et al.* (Particle Data Group), Phys. Rev. D **110**, 030001 (2024).
- [63] M. Fierz and W. Pauli, Proc. Roy. Soc. Lond. A **173**, 211 (1939).
- [64] D. G. Boulware and S. Deser, Phys. Rev. D **6**, 3368 (1972).
- [65] C. de Rham and G. Gabadadze, Phys. Rev. D **82**, 044020 (2010), arXiv:1007.0443 [hep-th].
- [66] C. de Rham, G. Gabadadze, and A. J. Tolley, Phys. Rev. Lett. **106**, 231101 (2011), arXiv:1011.1232 [hep-th].
- [67] S. F. Hassan and R. A. Rosen, JHEP **02**, 126 (2012), arXiv:1109.3515 [hep-th].
- [68] K. Hinterbichler and R. A. Rosen, JHEP **07**, 047 (2012), arXiv:1203.5783 [hep-th].
- [69] A. Schmidt-May and M. von Strauss, J. Phys. A **49**, 183001 (2016), arXiv:1512.00021 [hep-th].
- [70] J. M. Armaleo, D. López Nacir, and F. R. Urban, JCAP **09**, 031 (2020), arXiv:2005.03731 [astro-ph.CO].
- [71] K. Aoki and K.-i. Maeda, Phys. Rev. D **97**, 044002 (2018), arXiv:1707.05003 [hep-th].
- [72] E. Kun, Z. Keresztes, S. Das, and L. A. Gergely, Symmetry **10**, 520 (2018), arXiv:1905.04336 [astro-ph.CO].
- [73] D. Ganapathy *et al.* (LIGO O4 Detector), Phys. Rev. X **13**, 041021 (2023).
- [74] W. Jia *et al.* (members of the LIGO Scientific†), Science **385**, 1318 (2024), arXiv:2404.14569 [gr-qc].
- [75] E. Capote *et al.*, Phys. Rev. D **111**, 062002 (2025), arXiv:2411.14607 [gr-qc].
- [76] “O4a open data release,” <https://gwosc.org/O4/O4a/> (2025), accessed: November 3, 2025.
- [77] S. Karki *et al.*, Rev. Sci. Instrum. **87**, 114503 (2016), arXiv:1608.05055 [astro-ph.IM].
- [78] A. Viets *et al.*, Class. Quant. Grav. **35**, 095015 (2018), arXiv:1710.09973 [astro-ph.IM].
- [79] S. Soni *et al.* (LIGO), Class. Quant. Grav. **42**, 085016 (2025), arXiv:2409.02831 [astro-ph.IM].
- [80] E. Goetz and K. Riles, *Segments used for creating standard SFTs in O4 data*, Technical Note LIGO-T2400058-v1 (LIGO Laboratory, 2025) version v1; other version: LIGO-T2400058-v2.
- [81] O. J. Piccinni, P. Astone, S. D’Antonio, S. Frasca, G. Intini, P. Leaci, S. Mastrogiovanni, A. Miller, C. Palomba, and A. Singhal, Class. Quant. Grav. **36**, 015008 (2019), arXiv:1811.04730 [gr-qc].
- [82] P. Astone, S. Frasca, and C. Palomba, Class. Quant. Grav. **22**, S1197 (2005).
- [83] G. J. Feldman and R. D. Cousins, Phys. Rev. D **57**, 3873 (1998), arXiv:physics/9711021.
- [84] P. Astone, A. Colla, S. D’Antonio, S. Frasca, and C. Palomba, Physical Review D **90**, 042002 (2014).
- [85] N. Wiener *et al.*, *Extrapolation, interpolation, and smoothing of stationary time series: with engineering applications*, Vol. 8 (MIT press Cambridge, MA, 1964).
- [86] A. L. Miller, F. Badaracco, and C. Palomba (LIGO Scientific Collaboration, Virgo, KAGRA), Phys. Rev. D **105**, 103035 (2022), arXiv:2204.03814 [astro-ph.IM].
- [87] V. Rella, *Searching for ultra-light dark matter with gravitational-wave interferometers*, Master’s thesis (2021).
- [88] Y. Manita, K. Aoki, T. Fujita, and S. Mukohyama, Phys. Rev. D **107**, 104007 (2023), arXiv:2211.15873 [gr-qc].
- [89] C. Affeldt *et al.*, Class. Quant. Grav. **31**, 224002 (2014).
- [90] K. L. Dooley *et al.*, Class. Quant. Grav. **33**, 075009 (2016), arXiv:1510.00317 [physics.ins-det].
- [91] M. Maggiore, *Gravitational Waves: Volume 1: Theory and Experiments*, Vol. 1 (Oxford University Press, 2008).
- [92] M. Sereno and P. Jetzer, Mon. Not. Roy. Astron. Soc. **371**, 626 (2006), arXiv:astro-ph/0606197.
- [93] J. Murata and S. Tanaka, Class. Quant. Grav. **32**, 033001 (2015), arXiv:1408.3588 [hep-ex].

Appendix A: Transfer functions

In the dilaton search, we use transfer functions to relate the DM-induced fluctuations of the optics and the theorized coupling constants Λ_i^{-1} (see Eq. (1)). Following the approach in [22], we use detailed optical simulations in *Finesse* to calculate the transfer functions between the interferometer’s photodiode output amplitude and DM-induced fluctuations in the beamsplitter and arm test mirrors. The results, see Fig. 2, clearly show that in O4a, LLO is the more sensitive detector, with roughly a factor three gain in sensitivity (see Section VC) between O3 and O4a from the transfer function difference alone. At the same time, we also find that the performance of LHO has diminished over the same time period, though only slightly. In both cases, the differences are due to small changes in mirror thicknesses between the two runs.

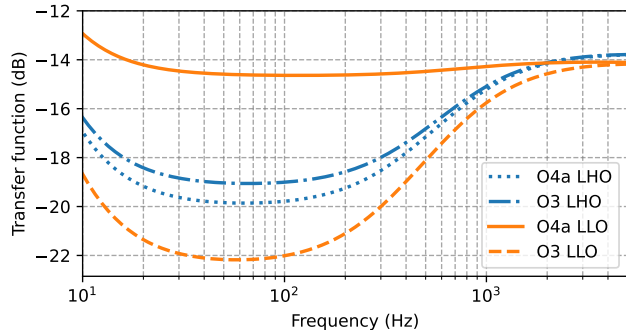


FIG. 2. Scalar dark matter transfer functions in dB, considering beamsplitter as well as arm test mirror size oscillations. The dotted lines show the LHO transfer functions, and the others show LLO results. As one can see, while the effect has reduced slightly in LHO between O3 and O4a, it has increased considerably in LLO, making LLO the more sensitive detector in O4a.